Current Optics and Photonics
Vol. 1, No. 4, August 2017, pp. 364-371

ISSN: 2508-7266(Print) / ISSN: 2508-7274(Online)
DOI: https://doi.org/10.3807/COPP.2017.1.4.364

Design and Manufacture of an Off-axis Aluminum Mirror for Visible-light Imaging

Jizhen Zhang[1,2], Xin Zhang[1]*, Shuanglong Tan[1], and Xiaolin Xie[1]

[1]*Key Laboratory of Optical System Advanced Manufacturing Technology, Changchun Institute of Optics, Fine Mechanics and Physics, Chinese Academy of Sciences, Changchun, Jilin 130033, China*
[2]*University of Chinese Academy of Sciences, Beijing 100049, China*

(Received October 22, 2016 : revised June 7, 2017 : accepted June 27, 2017)

Compared to one made of glass, an aluminum mirror features light weight, compact design, low cost, and quick manufacturing. Reflective mirrors and supporting structures can be made from the same material, to improve the athermal performance of the system. With the rapid development of ultraprecise machining technologies, the field of applications for aluminum mirrors has been developed rapidly. However, most of them are rotationally symmetric in shape, and are used for infrared applications. In this paper, the design and manufacture of an off-axis aluminum mirror used for a three-mirror-anastigmat (TMA) optical system at visible wavelengths is presented. An optimized, lightweight design provides a weight reduction of more than 40%, while the surface deformation caused by earth's gravity can meet the required tolerance. The two pieces of an off-axis mirror can be diamond-turned simultaneously in one setup. The centrifugal deformation of the off-axis mirror during single-point diamond turning (SPDT) is simulated through the finite-element method (FEM). The techniques used to overcome centrifugal deformation are thoroughly described in this paper, and the surface error is reduced to about 1% of the original value. After post-polishing, the form error is 1/30 λ RMS and the surface roughness is better than 5 nm Ra, which can meet the requirements for visible-light imaging.

Keywords : Metal mirror, Three-Mirror-Anastigmat (TMA), Single Point Diamond Turning (SPDT), Centrifugal deformation, Finite Element Method (FEM)
OCIS codes : (160.3900) Metals; (220.1920) Diamond machining; (220.4880) Optomechanics; (220.5450) Polishing

I. INTRODUCTION

Glassy materials such as borosilicate, fused silica, or glass ceramic are usually chosen for a mirror's substrate. The surface roughness of this kind of mirror can reach 1 nm RMS for a standard polish, and the low coefficients of thermal expansion of glassy materials minimize thermal distortion of mirrors. Besides, glassy materials often feature good dimensional stability [1]. However, there are some disadvantages of a glassy mirror substrate. First, the great difference in thermal coefficients of expansion between glassy mirror materials and conventional structural materials, such as aluminum and stainless steel, complicates opto-mechanical design to realize athermalization. Second, the thermal diffusivity of glass mirrors is often low, due to the poor thermal conductivity of these materials; it takes a long time for the optical system to reach thermal equilibrium, when a thermal gradient exists. Finally, glassy materials take a long time to grind and polish. In most cases this makes them the items with longest lead time in a project, and the fabrication cost of glass optics is high [2, 3].

Actually the first mirror appearing in human history was made from not glass, but metal. Supposedly it was a copper reflector, appearing about 6000 years ago. However, after the observation that glass with a thin metal coating is highly reflective, and besides other benefits is more scratch resistant, the use of metal mirrors decreased. In the last century, though, metal mirrors made a comeback, due to their

*Corresponding author: optlab@ciomp.ac.cn
Color versions of one or more of the figures in this paper are available online.

TABLE 1. Parameters of aluminum and some typical glass materials used for mirror substrates

Material	Specific stiffness	Thermal expansion	Thermal distortion index	Thermal diffusivity
	E/ρ (m^2/s^2)	α (K^{-1})	α/k (m/W)	$k/(\rho \cdot c_p)$ (m^2/s)
Aluminum alloy, 6061-T6	255×10^6	23.6×10^{-6}	141×10^{-9}	690×10^{-7}
Corning fused silica 7980	330×10^6	520×10^{-9}	400×10^{-9}	788×10^{-9}
Corning fused silica ULE 7972	307×10^6	30×10^{-9}	22.9×10^{-9}	776×10^{-9}
Schott zerodur	357×10^6	20×10^{-9}	68.5×10^{-9}	721×10^{-9}
Expectation	Large	Small	Small	Large

advantages for some new and interesting applications [4].

Traditional materials for metal mirrors in optical applications include aluminum, copper, and beryllium, and among them, the application of aluminum alloy is most extensive. Table 1 compares material parameters for aluminum alloy and typical glass materials used for mirror substrate [1]. In terms of mechanical properties, the specific stiffness of the aluminum alloy is equivalent to that of the glass material. Specific stiffness (the ratio of the elastic modulus E to the density ρ) is usually considered to be the criterion for evaluating the theoretical limit for making materials lightweight. In terms of thermal characteristics, the thermal performance of aluminum is better in most respects than that of glass, despite its higher coefficient of thermal expansion. The thermal distortion index of aluminum is less than that of fused silica 7980, and is surpassed only by low-thermal-expansion glasses like ULE and Zerodur. A smaller thermal distortion index indicates less distortion when the mirror is subject to a temperature gradient. The thermal diffusivity of aluminum is two orders of magnitude higher than that of glassy substrate, which means an aluminum mirror takes less time to reach thermal equilibrium under transient thermal loading conditions. Besides, an all-reflective optical system using aluminum in mirrors as well as structural components will not suffer from focus shifting when the temperature changes [5]. The lead time and manufacturing cost for aluminum mirrors are several times better than glass optics, due to the good machinability of metal materials. Meanwhile, more structural elements can be combined in the optomechanical design process of aluminum mirrors, which makes the whole system compact and easily assembled and tested.

At first, aluminum mirrors were used for infrared wavelengths and were not popular in spaceborne applications. The Wide-field Infrared Survey Explorer (WISE), a NASA Midex mission, is a cryogenic infrared observatory providing full-sky coverage of four infrared spectral bands from a sun-synchronous polar orbit. The 400-mm aperture telescope is an all-aluminum design, with aluminum mirrors mounted on an aluminum structure [6]. The RapidEye spacecraft was launched in 2008. The telescope optics are based on a TMA arrangement, with one spherical and two aspherical mirrors and a working spectrum from 440 nm to 850 nm. Its optical performance can be achieved by ultraprecise metal mirrors made of aluminum alloy Al6061-T6. The size of the primary mirror is around 210 × 190 mm. Deformation of the primary mirror caused by the NiP-Aluminium bimetallic effect is given; a homogeneous temperature change of 10 K generates different expansions of the aluminum base plate and NiP alloy. The deformation inside the quality area is 44.3 nm (p.-v.) and 6.9 nm (RMS), with a NiP layer 20 μm thick on the front and 40 μm thick on the back. Within 5 K of the operating temperature the maximum deformation would be 22 nm (p.-v.) [7]. The shape of most aluminum mirrors used in spaceborne applications are round or nearly square.

In this paper, design and manufacturing of an off-axis aluminum mirror for a TMA optical system used for visible light is presented. The length/width ratio of this rectangular mirror is nearly 3. FEM is used to predict the centrifugal deformation of the off-axis mirror during diamond turning. The surface deformation is reduced by a factor of 100, after adjusting rotational speed and adding auxiliary support at multiple points. Finally, the testing results for surface error and roughness are given.

II. DESIGN OF THE OFF-AXIS MIRROR FOR A TMA SYSTEM

2.1. Optical System

Off-axis TMA featuring a wide imaging field and no central obscuration has been widely used in optical systems [8]. The optical system presented in this paper is shown in Fig. 1. It is an F/4 off-axis Wetherell-TMA optical system

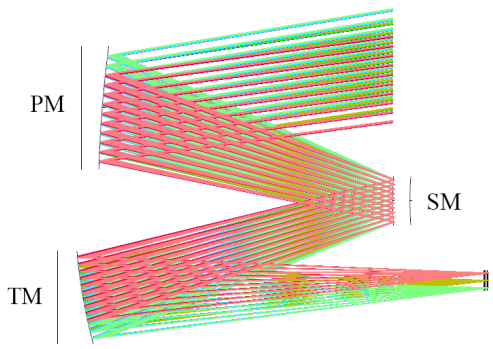

FIG. 1. Optical design of the TMA system.

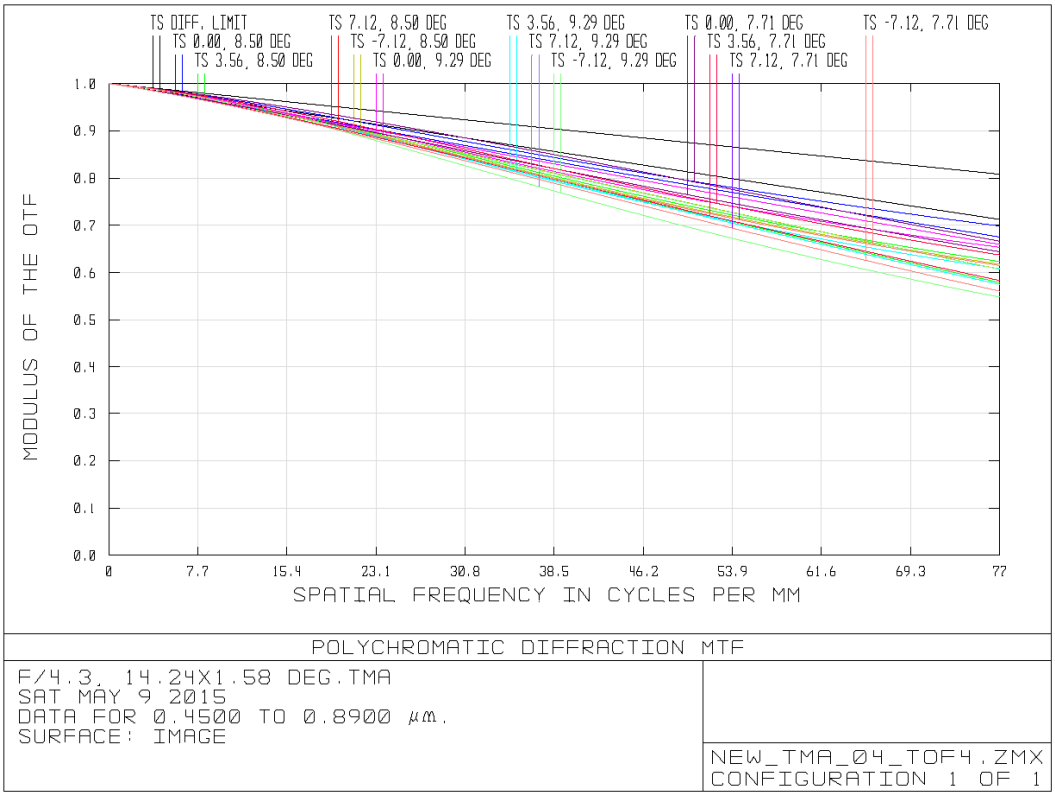

FIG. 2. MTF curves for the optical system.

with a focal length of 542 mm, working in the spectrum of 400-890 nm. The MTF curves of the optics, better than 0.550 for the whole field range, are given in Fig. 2.

The optical instrument is designed for a small satellite placed on a sun-synchronous, circular low-Earth orbit (LEO) of height 400 km. The telescope works with two large COMS detectors, each 12800 × 16 pixels. The pixel size of 6.5 × 6.5 μm defines a Nyquist frequency of ~77 lp/mm. The telescope can achieve a swath width of ~100 km with a pixel resolution of 5 × 5 m. The system that can achieve a 14.24° field of view consists of three reflective mirrors.

The primary mirror (PM) and tertiary mirror (TM) are off-axis aspherical, and the secondary mirror (SM), which defines and works as a stop, has a spherical shape. The secondary mirror is convex, with an effective aperture of 74 × 50 mm. Both PM and TM are rectangular and of similar size; one is 310 × 120 mm and the other is 280 × 100 mm. The rotational axes of all three mirrors are coincident. Since the SM is much smaller, and the other two mirrors with a length-width ratio share a similar design method, the TM is taken here as an example to present the design and manufacturing process for off-axis mirrors.

2.2. Design of Off-axis Mirror

The diameter/thickness ratio is an important design parameter that will affect the deformation and lightweight design of the mirror. Eq. (1) is Roberts' formula for selecting the diameter/thickness ratio of a solid flat plate [9].

$$\delta = \frac{3\rho g a^4}{16Et^2} = \frac{3\rho g \Delta^2 D^2}{256E} \tag{1}$$

δ : maximum deformation of the mirror, in m
ρ : material density, in kg/m^3
a : half aperture of the mirror, in m
E : elastic modulus of material, in MPa
t : thickness of the mirror, in m
Δ : diameter/thickness ratio

The mirror is made of 6061-T6 aluminum alloy and δ is defined to be 0.021 μm (1/30 λ, λ = 632.8 nm). According to Eq. (1), the value of Δ is 3.75.

Compared to glassy material, metals usually have good machinability, which makes the design of metal mirrors more flexible and diversified. A special lightweight design is adopted that provides a weight reduction of more than 40%. The polygonal holes parallel to the back side are

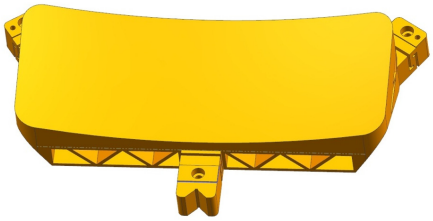

FIG. 3. CAD model of the tertiary mirror.

TABLE 2. Design results for the tertiary mirror

	Weight reduction rate	Size (mm)	Mass (kg)	Modal analysis (Hz)		
				First-order	Second-order	Third-order
Tertiary mirror	42%	280 × 100 × 65	2.25	705	909	1121

TABLE 3. Acceptable values for position errors of the TM

Errors	Acceptable value
ΔX (μm)	50
ΔY (μm)	50
ΘX (″)	12
ΘY (″)	12

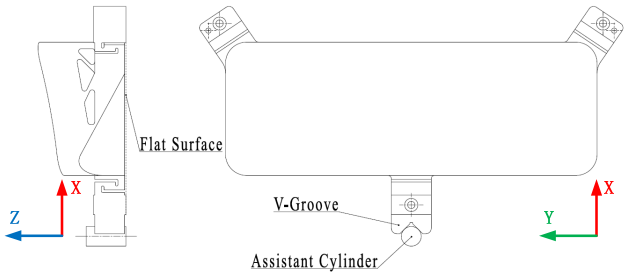

FIG. 4. Reference surfaces of the TM.

arranged in an orthogonal pattern. The distance between optical surface and holes is nearly constant, and optimized to avoid print-through effects. Figure 3 shows the CAD model of the TM. The positions of three independent foot points arranged around the mirror are also optimized, to realize minimal surface deformation under certain mechanical and thermal loads. To effectively isolate the installation stress and thermal stress from the optical surface, the flexible structure is carefully designed between the mounting surfaces and the reflective surface. Since stiffness is an important index of an optical mirror, modal analysis is given after the design of the weight-reducing holes and flexible structures. Table 2 gives the final design results for the TM.

The permissible position tolerance of the TM is shown in Table 3. These data are obtained through optical analysis.

As shown in Fig. 4, a flat surface and V-groove are designed as reference surfaces in the mirror to constrain the five degrees of freedom, with a cylinder as an assistant reference. The only unconstrained freedom is rotation about the *z*-axis. Two angular degrees of freedom are constrained by the flat surface, and the V-groove working with the assistant cylinder can constrain the other three linear degrees of freedom. The same structural elements are used during manufacturing and final assembly, which enables the position accuracy of the mirror to meet the tolerance.

2.3. Analyze of Gravity Deformation

Generally speaking, everything on the earth is affected by its gravity. For mirrors, gravity distortion can be divided into two parts. One is translation and rotation of the mirror relative to its original position; the other is surface deformation. Neither can be eliminated completely. However, as long as they are controlled within an acceptable range given by the optical designer, the requirements of an imaging system can be fulfilled. The finite-element method is effective for this kind of analysis, and the results are listed in Table 4. The worst case is in the *x*-direction, with gravity acting normal to the optical surface, and the movement and deformation in three directions are within the acceptable values.

III. MANUFACTURE OF THE OFF-AXIS ALUMINUM MIRROR

3.1. Single-point Diamond Turning

Aluminum mirrors can be diamond turned in a very efficient way. Making rotationally symmetric shapes such as spheres, aspheres, and off-axis aspheres is standard procedure for an SPDT machine. Even “free-form” mirrors can be manufactured under some special modes, like Slow

TABLE 4. Analysis results for gravity effects in three directions

Gravity direction		X	Y	Z	Acceptable value
Translation (μm)	ΔX	0.620	0.023	-0.002	50
	ΔY	0.040	0.257	-0.003	50
	ΔZ	-0.001	-0.001	0.340	50
Rotation (″)	θX	0.675	-0.048	-0.001	12
	θY	0.003	-0.002	0.1663	12
	θZ	6.833	-5.298	3.209	/
Surface deformation (nm RMS)		9.77	4.00	6.30	20

Tool Servo (STS) and Fast Tool Servo (FTS). Typical results that can be achieved are surfaces with a form irregularity around 70 nm RMS and microroughness better than 10 nm [10]. Figure 5 shows a SPDT machine with

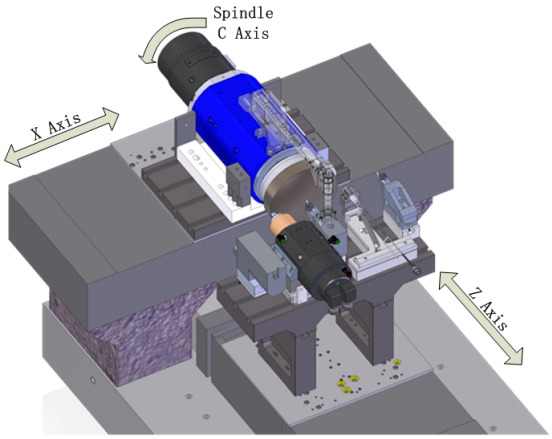

FIG. 5. Machine kinematics of a typical SPDT lathe.

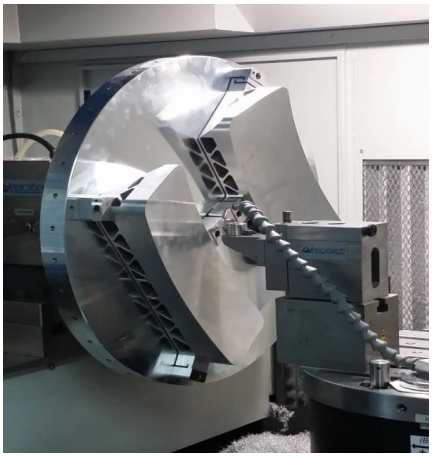

FIG. 6. SPDT of a pair of off-axis mirrors.

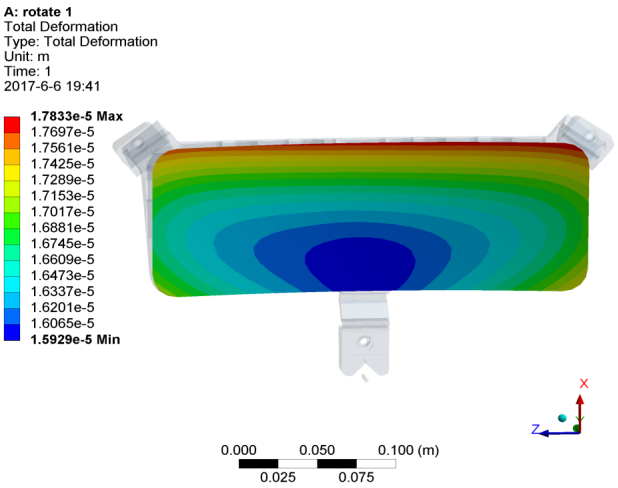

FIG. 7. Simulation of mirror deformation under centrifugal force.

two linear axes (X, Z) and one rotational axis (C). This machine can be used in 2-axis numerical controlling mode or 3-axis numerical controlling mode.

As mentioned above, the TM has a medium aperture size, and the off-axis distance is small. A very rigid work piece holder is used to mount two mirrors together. The diameter of the holder is about $\varphi = 420$ mm, which is under the maximum capability of the machine. Figure 6 shows the setup to machine tertiary mirrors. In this way, two mirrors can be manufactured simultaneously, and the balancing process can be much easier.

During the diamond turning, two pieces for the tertiary mirror are placed off-axis. The rotation generates a common centrifugal force that will deform the work pieces. Based on the finite-element method, it is possible to simulate the behavior of the mirror under manufacturing conditions. Figure 7 shows the simulated result under a typical rotational speed of 1500 rpm. The maximum deformation of the mirror is up to 18 μm, and the surface error cannot be measured by interferometer.

There are two possible ways to reduce the surface deformation caused by centrifugal effects. One is to reduce the centrifugal force generated by the turning process. Eq. (2) gives the formula for calculating centrifugal force.

$$F = \frac{\omega^2 \cdot r \cdot m}{2} \tag{2}$$

F: centrifugal force, in N
ω: rotational speed of the spindle, in rad/s
r: distance between barycenter of mirror and axis of rotation, in m
m: mass of the mirror, in kg

The above formula indicates that the centrifugal force F is directly proportional to ω^2, r and m. r and m are determined in the design process and cannot be adjusted during diamond turning. Reducing the rotational speed to a certain value is an effective method. When the rotational speed is reduced from 1500 to 500 rpm, the maximum surface deformation drops to 2 μm, about 1/10 as large as before. However, this value is still too large for the surface-measuring and post-polishing processes, and decreasing the rotational speed further will cause other problems.

Another way to overcome centrifugal force is by improving the overall stiffness of the working pieces. The stiffness of the mirror itself is determined once the design of the mirror is finished, so some auxiliary supporting methods can be used. The rule of thumb for a supporting plan is, do not induce extra stress in the mirror. First, the working holder for diamond turning has been carefully designed. The equivalent diameter D_E of the two TMs is about 400 mm, and a multiple-point supporting strategy is adopted to realize a uniform result. As shown in Fig. 8, the supporting area of each point is nearly the same, and there are 20 points in total, which can be divided into

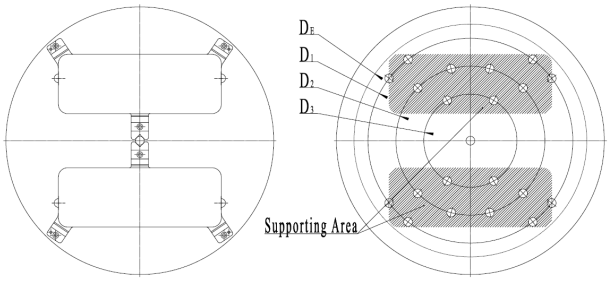

FIG. 8. Auxiliary supports at multiple points for the TM.

TABLE 5. Properties of four optical waxes

Wax	Softening temperature/°C	Adhesive strength	Density (10^3kg/m^3)
Slot	51	10	0.95
WT55H	55	27	/
Y-RW-99	55	35	1.03
C.S	72	80	1.72

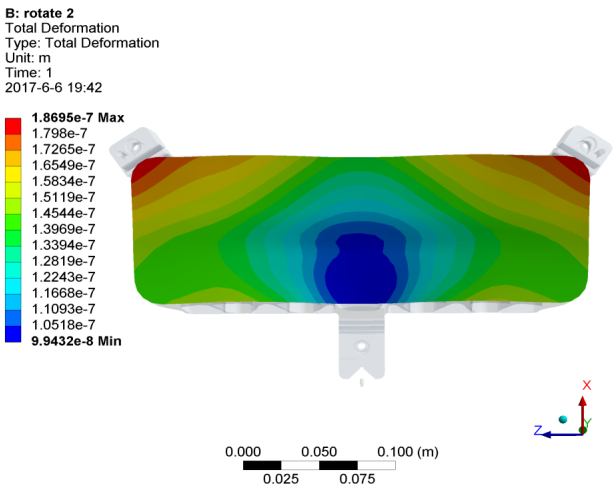

FIG. 9. Simulation of mirror deformation under centrifugal force, after adjustment.

three sets. Each set of points is distributed in one cycle, and the diameter of each distribution cycle can be calculated according to Eqs. (3)-(5).

$$D_1 = 0.4D_E \tag{3}$$

$$D_2 = 0.64D_E \tag{4}$$

$$D_3 = 0.88D_E \tag{5}$$

To avoid inducing extra stress, rigid connections are not used here. Some kinds of wax used in optical manufacturing are considered as candidates for soft connection between mirrors and holder. Table 5 gives the properties of some kinds of optical wax. In the end, WT55H, with a lower softening temperature and moderate adhesive force, has been chosen.

Figure 9 gives the simulated results after adjustment:, Deformation is reduced to 0.19 μm, which is about 1% of the original value. The result of testing after diamond turning is shown in Fig. 10: The surface error of the TM is nearly 1/10 λ RMS after diamond turning.

3.2. Post-polishing of the Mirror

Typical values for SPDT technology are around 0.1 μm for form error and 10 nm for surface roughness. This result is good enough for IR applications. However, shorter wavelengths, as for visible light, require higher accuracy in terms of both form error and microroughness. Diamond turning always produces microstructures, so-called turning structures. For applications in the visible spectrum, this periodic pattern has bad effects, similar to a diffraction grating [9]. Therefore, additional post-polishing must be employed, to improve the surface further. Unfortunately, aluminum is difficult to polish directly, because the material is not hard enough to be polished, and the grain structure determined by the crystalline metal itself limits the microroughness [11].

A layer of amorphous nickel-phosphorous (NiP), which is much harder than aluminum, is plated on the mirror

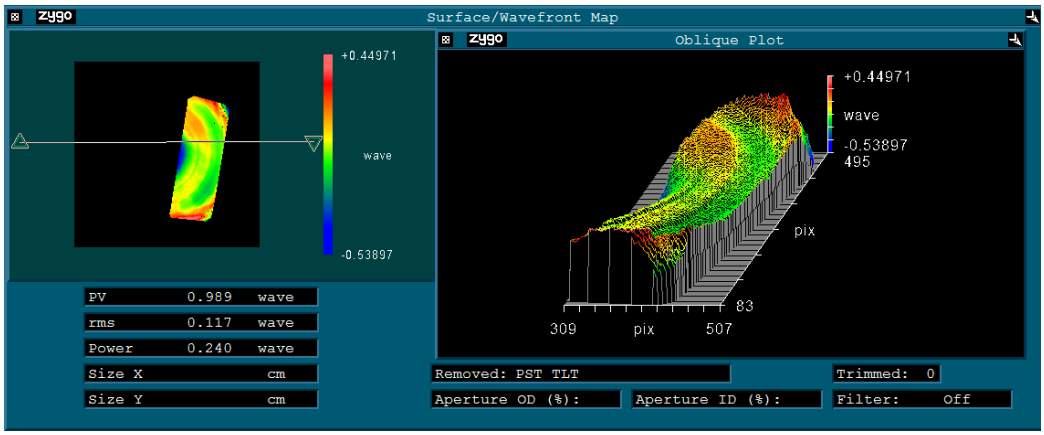

FIG. 10. Testing results after diamond turning.

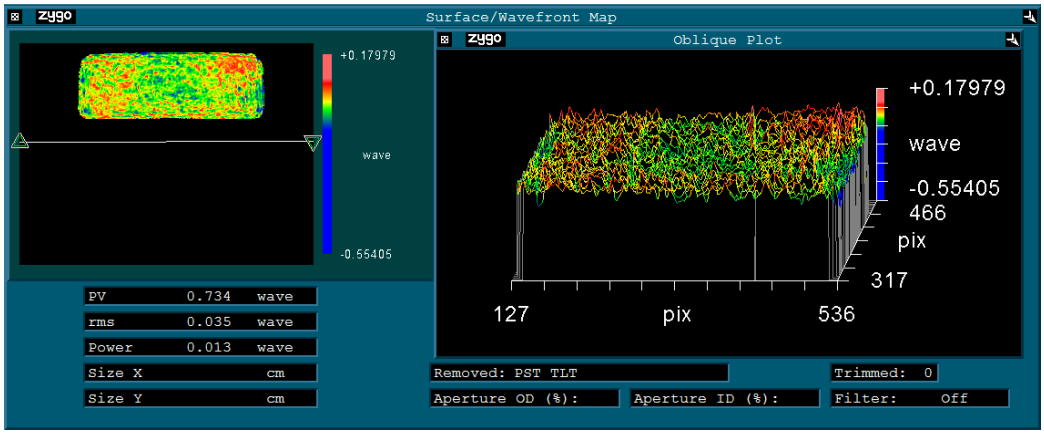

(a)

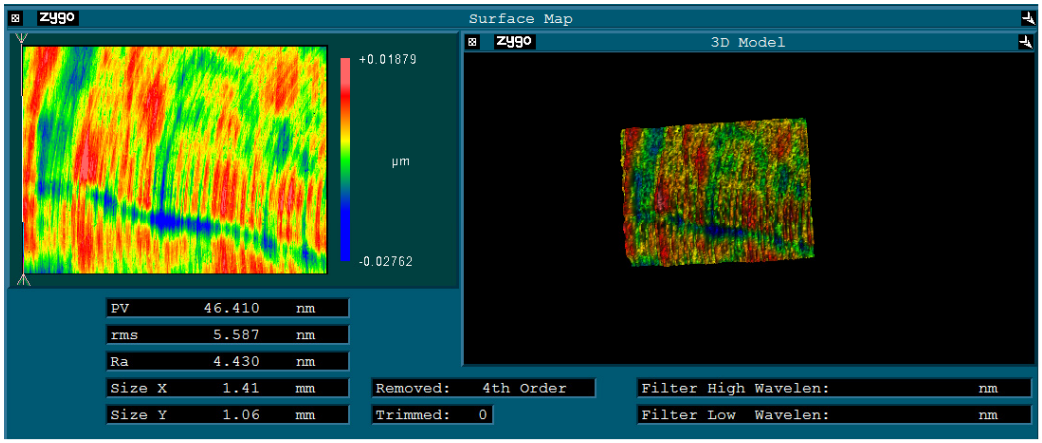

(b)

FIG. 11. (a) Form accuracy and (b) microroughness of the TM after post-polishing.

substrate. After plating, the mirror is diamond turned for a second time before polishing, so the minimum thickness of the layer should be larger than the cut depth of at least one loop. The post-polishing process can be applied in the traditional way, or computer-assisted. Figure 11 shows the results of testing the mirror after polishing. The form error is better than 1/30 λ RMS, and the surface roughness is better than 4 nm Ra.

IV. CONCLUSION AND FUTURE WORK

With its good material properties and machinability, aluminum provides a promising alternative mirror substrate to glassy materials for applications at visible wavelengths. The design and manufacturing of an off-axis aluminum mirror that acts as the tertiary mirror of a TMA system is presented in this paper. The aperture size of the mirror is 280 × 100 mm and the lightweight rate is over 40%. FEM is adopted to predict the surface deformation caused by centrifugal force during the single-point diamond turning process. The combination of SPDT and post-polishing technology improves the surface accuracy and microroughness of the reflective mirror to fulfill the requirements of VIS applications.

The other two mirrors (primary and secondary) are in the post-polishing process now. The supporting parts of the TMA system, which are also made of aluminum, are already finished. According to the agenda of this program, the whole system will be assembled and tested in the near future.

REFERENCES

1. D. Vukobratovich and J. P. Schaefer, "Large stable aluminum optics for aerospace applications," Proc. SPIE **8125**, 81250T (2011).
2. P. S. Carlin, "Lightweight mirror systems for spacecraft - an overview of materials & manufacturing needs," in *Proc. 2000 IEEE Aerospace Conf.*, pp. 169-181.
3. J. J. Guregian, J. W. Pepi, M. Schwalm, and F. Azad, "Material trades for reflective optics from a systems engineering perspective," Proc. SPIE **5179**, 85-96 (2003).
4. R. Steinkopf, A. Gebhardt, S. Scheiding, M. Rohde, O. Stenzel, S. Gliech, V. Giggel, H. Löscher, G. Ullrich, P. Rucks, A. Duparre, S. Risse, R. Eberhardt, and A. Tünnermann, "Metal

mirrors with excellent figure and roughness," Proc. SPIE **7102**, 71020C (2008).
5. T. H. Jamieson, "Athermalization of optical instruments from the optomechanical viewpoint," Proc. SPIE CR **43**, 131-159 (1992).
6. D. Sampath, A. Akerstrom, M. Barry, J. Guregian, M. Schwalm, and V. Ugolini, "The WISE telescope and scanner: design choices and hardware results," Proc. SPIE **7796**, 779609 (2010).
7. S. Risse, A. Gebhardta, C. Damma, T. Peschela, W. Stöckla, T. Feigla, S. Kirschsteinb, R. Eberhardta, N. Kaisera, and A. Tünnermanna, "Novel TMA telescope based on ultra precise metal mirrors," Proc. SPIE **7010**, 701016 (2008).
8. L. Clermont, Y. Stockman, W. Dierckx, and J. Loicq, "Comparison of off-axis TMA and FMA telescopes optimized over different fields of view: applications to Earth observation," Proc. SPIE **9131**, 91310N (2014).
9. F. Lei, Z. Yongzhi, and C. Yuyan, "Design and analysis of metal mirror for infrared off-axial system," Infrared Technol. **37**, 374-379 (2015).
10. M. N. Sweeney, "Advanced manufacturing technologies for light-weight post-polished snap-together reflective optical system designs," Proc. SPIE **4771**, 144 (2002).
11. S. Risse, A. Gebhardt, R. Steinkopf, and V. Giggel, "NiP plates mirrors for astronomy and space," in *Proc. of the 7th EUSPEN* (Bremen Congress Centre, German, May. 2007), pp. 348-351.